MetaCBT: A Multi-Layer Connectional Brain Template for Reproducible Population-Level Biomarker Discovery

Mayssa Soussia[1,2] *, Mohamed Ali Mahjoub[1], and Islem Rekik[2]

[1] National Engineering School of Sousse, University of Sousse, LATIS- Laboratory of Advanced Technology and Intelligent Systems, 4023, Sousse, Tunisia
[2] BASIRA Lab, Imperial-X and Department of Computing, Imperial College London, London, UK

Abstract. Connectional brain templates (CBTs) summarize population-level brain connectivity into a unified reference for studying neurodevelopmental disorders. All existing methods reduce the population to a *single* static connectivity matrix, discarding temporal dynamics, intra-block heterogeneity, and brain-state transition structure that carry disorder-specific information beyond any static estimate. We introduce **MetaCBT**, a framework that redefines the population template as a structured six-layer representation jointly encoding static inter-network coupling, dynamic variability, connectivity dispersion, dynamic lift (network-space projection of state-transition structure), co-activation bias, and transition grammar. Rather than averaging uniformly across subjects, MetaCBT anchors each population template to its most representative members through medoid-based weighting, requiring no supervision beyond the diagnostic labels already available. Evaluated on ABIDE-I, MetaCBT matches the discriminative accuracy of established single-layer baselines while producing markedly more reproducible biomarkers: the disorder-linked connectivity patterns it identifies remain far more stable across independent cross-validation folds than those recovered by any competing method. Crucially, layer ablation reveals a dissociation between classification-oriented and population-template-level discriminability, a structural property inaccessible to any single-layer representation. These results position multi-layer connectivity modeling as a more faithful and more reproducible foundation for biomarker discovery in heterogeneous neurodevelopmental conditions. Our source code is available at `https://github.com/basiralab/MetaCBT`.

Keywords: Connectional brain template · Multi-layer networks · Brain biomarkers · Biomarker reproducibility

1 Introduction

Brain connectivity provides a fundamental fingerprint of neural organization, capturing how distributed regions interact to support cognition and behavior [1,2].

* corresponding author: mayssa.soussia@hotmail.fr, `http://basira-lab.com`.

Connectional brain templates (CBTs) summarize a cohort into a single representative fingerprint to enable disease-related comparisons [3,4]. CBT learning has progressed from clustering-based averaging [5] to deep geometric learning. GNN methods such as DGN [6] and MGN-Net [7] replaced fixed aggregation with learned mappings over heterogeneous connectomes [8], while hypergraph and reservoir-based frameworks [9,10,11] extended CBTs to higher-order interactions and cognitively enhanced templates. Despite this progress, one assumption has remained constant: the population is reduced to a *single* connectivity template, creating four representational limitations. (i) *Temporal variability is absent*: within-scan FC fluctuations carry clinical information [12] that is lost upon aggregation. (ii) *Intra-block heterogeneity is discarded*: brain organization spans multiple spatial scales [13,14] no single matrix can jointly express. (iii) *State-transition structure is unrepresented*: connectivity reorganizes in structured temporal sequences [15] with no mechanism for encoding in a static template. (iv) *Transient co-activation structure is invisible*: networks that jointly enter high-activity states more or less often than expected under independence carry coalition-level information absent from average coupling strength. These limitations are consequential in neurodevelopmental conditions such as ASD, where connectivity alterations are distributed and heterogeneous [16,17].

We introduce **MetaCBT**, a framework that redefines the CBT from a single connectivity matrix into a structured multi-layer representation preserving complementary dimensions of functional organization. Our contributions are threefold. (1) We propose a multi-layer CBT formulation encoding complementary static, dynamic, and state-transition connectivity dimensions, together with a medoid-proximity estimation strategy that anchors the template to the most representative class members. (2) We demonstrate that this representation yields significantly more reproducible ASD biomarkers than conventional single-layer CBTs while maintaining comparable classification performance. (3) Through systematic layer ablation, we reveal complementary disorder signatures that remain hidden in any individual connectivity layer, providing a more interpretable characterization of disorder-specific brain organization. We hypothesize that integrating complementary connectivity dimensions into a single population template improves biomarker reproducibility while preserving discriminative power.

2 Method

Fig. 1 summarizes the MetaCBT pipeline: raw fMRI is mapped to a six-layer subject representation (Sect. 2.1), subjects are aggregated into a medoid-weighted population template (Sect. 2.2), and the resulting templates are evaluated for cross-fold biomarker reproducibility (Sect. 3).

2.1 Multi-scale subject representation

Let $\mathcal{D}=\{(X_i, y_i)\}_{i=1}^{N}$, where $X_i \in \mathbb{R}^{T_i \times N_r}$ is the resting-state fMRI time series (T_i time points, N_r ROIs, $y_i \in \{0, 1\}$). ROIs are grouped into Q functional networks

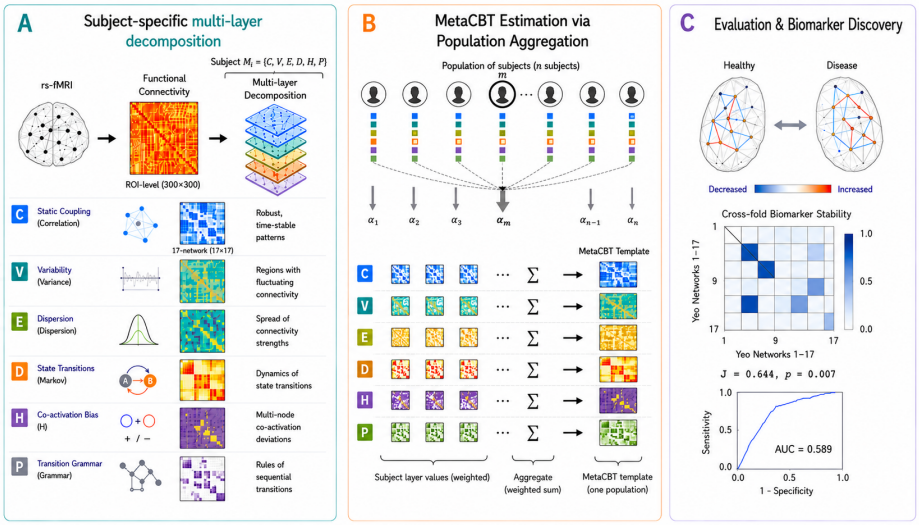

Fig. 1. MetaCBT framework overview. (A) Resting-state fMRI is mapped to six complementary connectivity layers: static coupling (C), dynamic variability (V), dispersion (E), dynamic lift (D), co-activation bias (H), and transition grammar (P). (B) Medoid-proximity weights aggregate all subjects across all six layers into a structured class-level multi-layer template. (C) Cross-fold Jaccard quantifies biomarker reproducibility.

via a parcellation atlas. The static ROI-level FC matrix $R_i = \mathrm{corr}(X_i) \in \mathbb{R}^{N_r \times N_r}$ and a sequence of windowed FC matrices $\{F_i^{(w)}\}_{w=1}^{W_i}$ together yield the six-layer subject representation $M_i = \{C_i, V_i, E_i, D_i, H_i, P_i\}$, where $C, V, E, D, H \in \mathbb{R}^{Q \times Q}$ and $P_i \in \mathbb{R}^{K \times K}$ (K shared brain states). All matrix layers are symmetrized.

Layer C: inter-network coupling. Layer C summarizes the mesoscale static connectivity between functional systems by block-averaging ROI-level correlations:

$$C_i(a,b) = \frac{1}{|G_a|\,|G_b|} \sum_{u \in G_a} \sum_{v \in G_b} R_i(u,v), \tag{1}$$

where G_a and G_b denote the sets of ROIs belonging to networks a and b, respectively. This layer provides the static backbone of large-scale functional organization against which dynamic layers are contrasted.

Layer V: dynamic variability. Layer V captures temporal fluctuations in functional coupling by computing, for each network pair, the interquartile range (IQR) of windowed coupling estimates across time:

$$V_i(a,b) = \mathrm{IQR}_w\big(\bar{F}_i^{(w)}(a,b)\big) \cdot \min\left(1, \left(\frac{W_i}{W_{\mathrm{ref}}}\right)^{\beta}\right), \tag{2}$$

where $\bar{F}_i^{(w)}(a,b)$ denotes the mean windowed coupling between networks a and b in window w, obtained by block-averaging $F_i^{(w)}$ analogously to Eq. (1); W_{ref}

is a population-level reference window count, and $\beta \in (0, 1)$ is a scan-length correction exponent. The correction shrinks variability estimates for subjects with fewer windows, so that differences in scan duration do not confound cross-subject comparisons.

Layer E: connectivity dispersion. Layer E quantifies within-block spatial heterogeneity using the coefficient of variation of absolute ROI-level correlations within each network-pair block:

$$E_i(a, b) = \frac{\mathrm{std}\big(|R_i^{ab}|\big)}{\mathrm{mean}\big(|R_i^{ab}|\big) + \varepsilon}, \tag{3}$$

where R_i^{ab} is the sub-matrix of R_i restricted to networks a and b, and $\varepsilon > 0$ prevents division by zero.

Layer D: dynamic lift. To represent how network interactions are shaped by brain-state transition dynamics, we introduce the dynamic lift. Windowed connectivity patterns from all subjects are clustered into K shared brain states (Fig. 2) using a population-level procedure. Each subject is characterized by a network-by-state engagement matrix $B_i \in \mathbb{R}^{Q\times K}$, where $B_i(a, k)$ is the mean absolute coupling of network a to state centroid k, and a row-stochastic Markov transition matrix $\Pi_i \in \mathbb{R}^{K\times K}$. The dynamic lift projects state-transition structure back into network space:

$$D_i = B_i\, \Pi_i\, B_i^{\top} \in \mathbb{R}^{Q\times Q}, \tag{4}$$

where $D_i(a, b)$ encodes how strongly networks a and b co-engage through the sequence of brain-state transitions, a quantity absent from any static or time-averaged FC measure.

Layer H: co-activation bias. Layer H captures transient network coalition structure by measuring statistical deviations from independent network recruitment. For each window, the top-k most active networks are identified by their mean absolute coupling strength. The co-activation bias between networks a and b is:

$$H_i(a, b) = \Pr(a, b \text{ active}) - \Pr(a \text{ active})\ \Pr(b \text{ active}), \tag{5}$$

where probabilities are estimated empirically from the windowed sequence. Positive values indicate that a and b co-recruit more frequently than expected under independence; negative values indicate mutual suppression. This layer is complementary to Layer C: while C captures average coupling strength, H captures the tendency of networks to jointly enter high-activity states.

Layer P: transition grammar. Layer P retains the full subject-specific Markov matrix $P_i = \Pi_i \in \mathbb{R}^{K\times K}$, $P_i(k, \ell) = \Pr(s_{t+1}{=}\ell \mid s_t{=}k)$, encoding the temporal grammar of brain-state switching. Layers D and P share the same decomposition but are non-redundant: D projects transition structure into *network space* $(Q\times Q)$, capturing which network pairs are dynamically coupled through state sequences; P retains it in *state space* $(K \times K)$, capturing the persistence and sequencing of states themselves.

2.2 Template estimation

For a population y with training subjects S_y, the MetaCBT template is defined as $\mathcal{T}_y = \{\mathcal{T}_y^\ell\}_{\ell \in \{C,V,E,D,H,P\}}$, where each layer ℓ encodes a distinct connectivity view. To ensure robustness to inter-subject variability and outliers, each feature dimension is normalized within the training fold using a robust scaling scheme based on the median and median absolute deviation (MAD). Specifically, for each layer ℓ, we compute $\mathrm{MAD}(x) = \mathrm{median}\big(|x - \mathrm{median}(x)|\big)$, and use it alongside the median to obtain outlier-resistant standardized embeddings: $\{\tilde{v}_i^\ell\}$.

Medoid-based subject weighting. To construct a robust population template, we assign higher importance to subjects that are more representative of the group. We first obtain a joint static–dynamic embedding for each subject by concatenating complementary layer representations, $z_i = [\tilde{v}_i^C; \tilde{v}_i^V]$. We define a medoid subject $m_y = \arg\min_{j \in S_y} \sum_{i \in S_y} \|z_i - z_j\|_2$, which serves as the most central example in the population space. Each subject is then assigned a weight based on its distance to the medoid, so that closer subjects contribute more while outliers are down-weighted. Finally, layer-specific templates are computed as a weighted average of subject-level representations (for correlation-based connectivity, we apply Fisher-z averaging).

3 Results

Dataset and evaluation. ABIDE-I [18]: 215 subjects (99 ASD, 116 TD) after excluding 25 with fewer than 12 valid sliding windows. Functional time series were extracted using 300 Schaefer ROIs [19] grouped into 17 Yeo networks [20]. All experiments use stratified 5-fold CV. Templates and normalization statistics are estimated from the training split only and applied frozen to held-out subjects, ensuring no leakage across folds. Bootstrap CIs use 400 resamples; permutation tests use 200 label-permuted runs.

Multi-layer MetaCBT. Fig. 2 shows MetaCBT-Standard templates for ASD and TD. All six layers exhibit distinct spatial profiles, consistent with each encoding a different aspect of connectivity organization. Layer D shows the most spatially structured ASD–TD divergence, with state-transition coupling reductions at frontoparietal (network 6) and somatomotor/temporoparietal (networks 8–9) regions; Layer C reveals systematic Default Mode–Salience Ventral Attention hypoconnectivity.

Biomarker reproducibility. MetaCBT's primary contribution is the reproducibility of the disorder-linked connectivity alterations it identifies, assessed on the medoid-weighted Layer-C (static coupling) template. We measure this by the mean pairwise cross-fold Jaccard index over the top-10 discriminative network pairs, ranked by the Layer-C template difference $|\Delta T^C|$, across all fold pairs:

$$J = \frac{1}{10} \sum_{i<j} \frac{|\mathcal{P}_i \cap \mathcal{P}_j|}{|\mathcal{P}_i \cup \mathcal{P}_j|}, \tag{6}$$

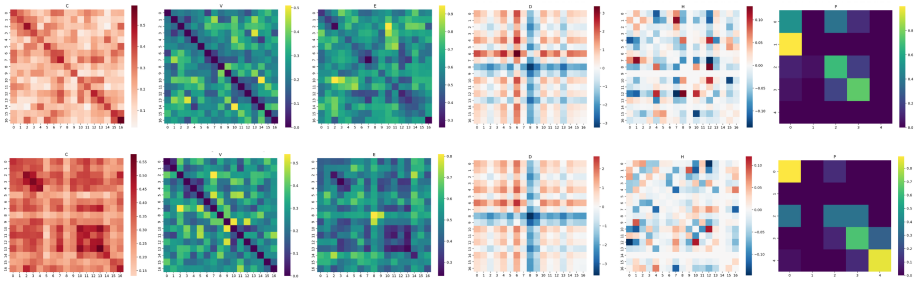

Fig. 2. MetaCBT-Standard templates (ASD top, TD bottom) across all six layers. Layers C–H: 17×17 network matrices. Layer P: 5×5 brain-state transition matrix. Distinct spatial profiles across layers confirm non-redundant population encoding.

where $\mathcal{P}_f$ is this top-10 set in fold f, and significance is assessed against 200 label-permuted runs.

Table 1 reports Jaccard stability for all methods. MetaCBT achieves J=**0.644** (p=0.007, 95% CI on the permuted-null mean $[0.000, 0.020]$), the highest of all evaluated methods, exceeding baselines by 0.10–0.16 Jaccard units, including the nearest baseline (Gen-HNN: 0.542, p=0.010). All methods exceed their respective label-permuted nulls, confirming that template-based biomarker selection is generally stable at this sample size; MetaCBT's advantage reflects medoid-weighted aggregation anchoring the template to the most representative subjects.

Table 1. Cross-fold biomarker stability (ABIDE, top-10 discriminative network pairs, 5-fold CV). J: mean pairwise Jaccard. Null: mean of 200 label-permuted runs. p-values one-sided empirical.

Method	J	Null	p
MetaCBT-Std	**0.644**	0.446	**0.007**
DGN [6]	0.486	0.257	0.025
Gen-HNN [10]	0.542	0.256	0.010
mCOCO [9]	0.533	0.267	0.007

Table 2 lists the five most discriminative network pairs. All show ASD<TD coupling. DefaultA–SalVentAttnA ($|\Delta T^C|$=0.315) and four runners-up converge on Default Mode–Salience Ventral Attention and Default–Somatomotor interactions, consistent with meta-analyses of ASD functional connectivity [21,22].

Fig. 3 visualizes cross-fold stability across all 17×17 network pairs: bright cells identify pairs that appear consistently in the top-10 discriminative set across all five folds, while dark cells appear rarely or never. Stable signal concentrates on SomMotB–TempPar (indices 8–9) and SalVentAttn–DefaultA (indices 10–12) interactions, corroborating the ranked pairs in Table 2 and confirming that

Table 2. Top-5 discriminative network pairs (ABIDE, MetaCBT-Standard), ranked by $|\Delta T^C|$. All pairs ASD<TD. Ranks 2–5 differ by <0.004; ordering may not generalize.

Rk.	Network A	Network B	$\lvert\Delta T^C\rvert$
1	DefaultA	SalVentAttnA	0.315
2	DefaultA	SalVentAttnB	0.281
3	SalVentAttnB	TempPar	0.281
4	DefaultA	SomMotB	0.280
5	DefaultB	SalVentAttnB	0.278

MetaCBT's Jaccard gain reflects a genuine narrowing of the discriminative set rather than arbitrary ranking variation.

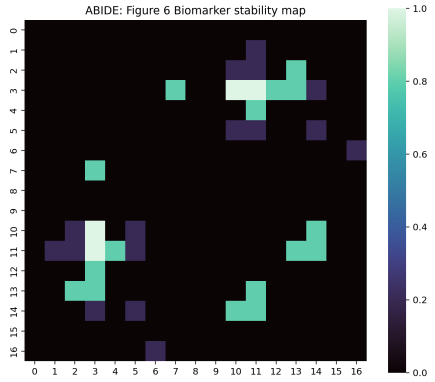

Fig. 3. Cross-fold biomarker stability map: frequency of each network pair among the top-10 discriminative set across five CV folds (Yeo-17 axes, index 0 = VisCent through 16 = DefaultC). Stable pairs concentrate in SomMotB–TempPar and SalVentAttn–DefaultA regions. Mean pairwise Jaccard J=0.644 (p=0.007 vs. label-permuted null).

Classification performance. Table 3 reports template-based classification. MetaCBT-Standard achieves BA=0.586 (95% CI $[0.516, 0.651]$, permutation p=0.015) and AUC=0.589 ($[0.507, 0.663]$). Pairwise BA differences span 0.000–0.013 with overlapping CIs, consistent with comparable discriminative performance across methods. MetaCBT achieves the highest template-separation margin, indicating superior class-template separation in the normalized distance space despite equivalent classification accuracy. These results confirm that multi-layer enrichment does not sacrifice discriminative power.

Layer contribution analysis. Table 4 reports single-layer ablations. The full six-layer MetaCBT-Standard (BA=0.586) outperforms all single-layer configurations, indicating that the layers encode complementary rather than redundant

Table 3. Template-based classification on ABIDE (n=215, 5-fold CV, linear SVM). Pairwise BA differences 0.000–0.013; all CIs overlap. Margin: mean normalized distance to incorrect minus correct template (higher is better). †Re-implemented approximation.

Method	BA	95% CI	AUC	95% CI	Margin
MetaCBT-Std	**0.586**	[0.516, 0.651]	0.589	[0.507, 0.663]	**0.107**
DGN [6]†	0.571	[0.500, 0.638]	0.598	[0.527, 0.670]	0.013
Gen-HNN [10]†	0.573	[0.507, 0.642]	0.603	[0.526, 0.683]	0.020
mCOCO [9]†	0.585	[0.517, 0.653]	0.604	[0.526, 0.688]	0.020

Table 4. Layer ablation (ABIDE). ALL=MetaCBT-Standard. ΔT_{Fro}: Frobenius norm of the layer-specific ASD−TD difference template (template-level discriminability). Single-layer models use only the stated layer for template construction and classification.

Model	BA	AUC	Margin	ΔT_{Fro}
ALL (MetaCBT-Std)	**0.586**	**0.589**	**0.107**	—
V (variability)	0.547	0.524	0.035	1.727
C (mean coupling)	0.528	0.537	0.021	2.249
H (co-activation)	0.525	0.507	0.006	0.931
E (dispersion)	0.520	0.535	−0.052	3.041
D (dynamic-lift)	0.473	0.488	−0.004	**3.949**
P (grammar)	0.440	0.445	−0.166	1.514

disorder-related information. The ablation reveals a **V–D dissociation** between classification-oriented and template-level discriminability. Layer V achieves the highest single-layer BA (0.547) yet carries the lowest template-level ASD–TD divergence by Frobenius norm (ΔT_{Fro}=1.727). Conversely, Layer D produces the largest template-level divergence (ΔT_{Fro}=3.949) yet the second-lowest single-layer BA (0.473). This reveals two complementary discrimination modes: dynamic variability (V) encodes disorder signal primarily in the *subject-to-template distance space* (individual sensitivity); the dynamic lift (D) encodes the largest population-level disorder signature at the *template level* (population specificity). Neither mode replicates the combined result, supporting the six-layer design. Layers D and P perform below chance as standalone classifiers (BA=0.473 and 0.440, respectively). This pattern is consistent with these layers' disorder signal being expressed primarily at the population-template level rather than as subject-level scalar distance; we do not directly isolate their marginal contribution within the fused model. We interpret this as a property of the architecture rather than a limitation.

4 Conclusion

We introduced MetaCBT, a multi-layer formulation of the connectional brain template that jointly encodes static, dynamic, and state-transition structure rather than collapsing connectivity into a single matrix. By combining medoid-proximity subject weighting with a structured multi-layer template representation, it yields population fingerprints that are more representative, discriminative, and reproducible than single-layer alternatives. The V–D dissociation observed under layer ablation highlights a key result: complementary disorder-specific signals emerge only through multi-layer integration. Overall, these findings support structured, multi-scale representations of brain connectivity as a more informative direction for biomarker discovery in heterogeneous neurodevelopmental conditions.

References

1. Finn, E.S., Shen, X., Scheinost, D., Rosenberg, M.D., Huang, J., Chun, M.M., Papademetris, X., Constable, R.T.: Functional connectome fingerprinting: identifying individuals using patterns of brain connectivity. Nature Neuroscience **18** (2015) 1664–1671
2. L, S.M., Tian, Y., Yeo, B., Cropley, V., Zalesky, A.: High-resolution connectomic fingerprints: Mapping neural identity and behavior. NeuroImage (2021) 117695
3. Dhifallah, S., Rekik, I.: Estimation of connectional brain templates using selective multi-view network normalization. Medical Image Analysis **62** (2020) 101567
4. Mhiri, I., Rekik, I.: Joint functional brain network atlas estimation and feature selection for neurological disorder diagnosis. Medical Image Analysis **60** (2020) 101596
5. Dhifallah, S., Rekik, I.: Clustering-based multi-view network fusion for estimating brain network atlases of healthy and disordered populations. Journal of Neuroscience Methods **311** (2019) 426–435
6. Gurbuz, M.B., Rekik, I.: Deep graph normalizer: A geometric deep learning approach for estimating connectional brain templates. In: MICCAI. (2020)
7. Gurbuz, M.B., Rekik, I.: Mgn-net: A multi-view graph normalizer for integrating heterogeneous biological network populations. Medical Image Analysis **71** (2021) 102059
8. Bessadok, A., Mahjoub, M.A., Rekik, I.: Graph neural networks in network neuroscience. IEEE Transactions on Pattern Analysis and Machine Intelligence **45** (2023) 5833–5848
9. Soussia, M., Mahjoub, M.A., Rekik, I.: Multi-sensory cognitive computing for learning population-level brain connectivity. In: International Conference on Medical Image Computing and Computer-Assisted Intervention, Springer (2025) 521–531
10. Soussia, M., Mahjoub, M.A., Rekik, I.: Generative hypergraph neural network for multiview brain connectivity fusion. In: PRIME Workshop, MICCAI. (2024)
11. Soussia, M., Mahjoub, M.A., Rekik, I.: Hypercoco: Multi-sensory hyper cognitive computing for learning population level brain connectivity. Medical Image Analysis **113** (2026) 104156
12. Hutchison, R.M., Womelsdorf, T., Allen, E.A., Bandettini, P.A., Calhoun, V.D., Corbetta, M., Della Penna, S., Duyn, J.H., Glover, G.H., Gonzalez-Castillo, J., Handwerker, D.A., Keilholz, S., Kiviniemi, V., Leopold, D.A., de Pasquale, F.,

Sporns, O., Walter, M., Chang, C.: Dynamic functional connectivity: Promise, issues, and interpretations. NeuroImage **80** (2013) 360–378
13. Betzel, R.F., Bassett, D.S.: Multi-scale brain networks. NeuroImage **160** (2017) 73–83
14. Meunier, D., Lambiotte, R., Bullmore, E.: Modular and hierarchically modular organization of brain networks. Frontiers in Neuroscience **4** (2010)
15. Vidaurre, D., Smith, S.M., Woolrich, M.W.: Brain network dynamics are hierarchically organized in time. Proceedings of the National Academy of Sciences **114** (2017) 12827–12832
16. Hull, J.V., Dokovna, L.B., Jacokes, Z.J., Torgerson, C.M., Irimia, A., Van Horn, J.D.: Resting-state functional connectivity in autism spectrum disorders: A review. Frontiers in Psychiatry **7** (2017) 205
17. Konrad, K., Eickhoff, S.B.: Is the adhd brain wired differently? a review on structural and functional connectivity in attention deficit hyperactivity disorder. Human Brain Mapping **31** (2010) 904–916
18. di Martino, A., Yan, C.G., Li, Q., Denio, E., Castellanos, F., Alaerts, K., Anderson, J.S., Assaf, M., Bookheimer, S., Dapretto, M., Deen, B., Delmonte, S., Dinstein, I., Ertl-Wagner, B., Fair, D.A., Gallagher, L., Kennedy, D.P., Keown, C., Keysers, C., Lainhart, J., Lord, C., Luna, B., Menon, V., Minshew, N.J., Monk, C.S., Mueller, S., Müller, R.A., Nebel, M.B., Nigg, J., O'Hearn, K., Pelphrey, K.A., Peltier, S.J., Rudie, J.D., Sunaert, S., Thioux, M., Tyszka, J., Uddin, L., Verhoeven, J., Wenderoth, N., Wiggins, J., Mostofsky, S., Milham, M.: The autism brain imaging data exchange: Towards large-scale evaluation of the intrinsic brain architecture in autism. Molecular psychiatry **19** (2013) 659 – 667
19. Schaefer, A., Kong, R., Gordon, E.M., Laumann, T.O., Zuo, X., Holmes, A., Eickhoff, S., Yeo, B.T.T.: Local-global parcellation of the human cerebral cortex from intrinsic functional connectivity mri. bioRxiv (2017)
20. Yeo, B.T., Krienen, F.M., Sepulcre, J., Sepulcre, J., Sabuncu, M., Sabuncu, M., Lashkari, D., Hollinshead, M.O., Hollinshead, M.O., Roffman, J., Smoller, J., Zöllei, L., Polimeni, J., Fischl, B., Fischl, B., Liu, H., Buckner, R.L.: The organization of the human cerebral cortex estimated by intrinsic functional connectivity. Journal of neurophysiology **106 3** (2011) 1125–65
21. Hull, J.V., Dokovna, L.B., Jacokes, Z.J., Torgerson, C., Irimia, A., Horn, J.V.V.: Resting-state functional connectivity in autism spectrum disorders: A review. Frontiers in Psychiatry **7** (2017)
22. Cerliani, L., Mennes, M., Thomas, R., di Martino, A., Thioux, M., Keysers, C.: Increased functional connectivity between subcortical and cortical resting-state networks in autism spectrum disorder. JAMA psychiatry **72** (2015) 767 – 777